Size-Dependent Energy Levels of InSb Quantum Dots Measured by Scanning Tunneling Spectroscopy

Tuo Wang,[†] Roman Vaxenburg,[‡] Wenyong Liu,[†] Sara M. Rupich,[†] Efrat Lifshitz,[‡] Alexander L. Efros,[§] Dmitri V. Talapin,[*,†] and S. J. Sibener[*,†]

[†]The James Franck Institute and Department of Chemistry, The University of Chicago, Chicago, Illinois 60637, United States, [‡]Schulich Faculty of Chemistry, Technion - Israel Institute of Technology, Haifa 32000, Israel, and [§]Center for Computational Material Science, Code 6390 Naval Research Laboratory, Washington D.C. 20375, United States

ABSTRACT The electronic structure of single InSb quantum dots (QDs) with diameters between 3 and 7 nm was investigated using atomic force microscopy (AFM) and scanning tunneling spectroscopy (STS). In this size regime, InSb QDs show strong quantum confinement effects which lead to discrete energy levels on both valence and conduction band states. Decrease of the QD size increases the measured band gap and the spacing between energy levels. Multiplets of equally spaced resonance peaks are observed in the tunneling spectra. There, multiplets originate from degeneracy lifting induced by QD charging. The tunneling spectra of InSb QDs are qualitatively different from those observed in the STS of other III–V materials, for example, InAs QDs, with similar band gap energy. Theoretical calculations suggest the electron tunneling occurs through the states connected with *L*-valley of InSb QDs rather than through states of the Γ-valley. This observation calls for better understanding of the role of indirect valleys in strongly quantum-confined III–V nanomaterials.

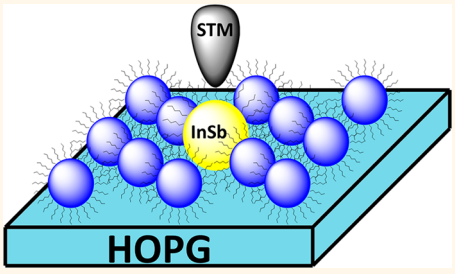

KEYWORDS: quantum dots · scanning tunneling spectroscopy · InSb · electronic structure · electron tunneling

Recent developments of chemical synthesis enabled preparation of size series of different semiconductor materials in the form of monodisperse nanocrystals (NCs).[1] Strong spatial confinement of electrons and holes in sub-10 nm NCs results in the atomic-like discrete states whose energy depends on the NC size. In nearly spherical NCs, often referred to as quantum dots (QDs), these states show *S*, *P*, *D*, *etc.* symmetries analogous to the corresponding atomic orbitals. By controlling the size, shape, and materials of the QDs during synthesis, the electronic states can be tuned toward achieving the desired optical and electronic properties.[2,3] Chemically synthesized QDs can also serve as building blocks to form more complex structures such as two- or three-dimensional superlattices.[4–7]

Indium antimonide (InSb), a narrow-gap semiconductor from the III–V group, is an important material for modern semiconductor industry. Bulk InSb is used in infrared detectors because of its sensitivity in the mid-IR region up to 5 μm. InSb is also used in terahertz radiation sources due to its high electron mobility. Recently, colloidal InSb NCs with different sizes have been successfully synthesized by colloidal chemistry.[8] Optical absorption spectroscopy of InSb NCs shows well resolved excitonic transitions in the near-infrared region. These transitions, which inherently involved two energy states, cannot be used to access individual energy levels or separately investigate conduction and valence bands. Moreover, optical spectroscopy is subject to quantum selection rules, which forbid some transitions from being seen.

In this work, we present a scanning probe microscopy (SPM) and scanning tunneling spectroscopy (STS) of the electronic properties of single, isolated InSb QDs over a size range of 3–7 nm. The STS technique provides information on the electron and hole level structures of the QD by accessing all energy states directly and probing the local density of electronic states (LDOS).[9–16] The observed tunneling spectra of the conduction band show eight resonance peaks

* Address correspondence to s-sibener@uchicago.edu, dvtalapin@uchicago.edu.

Received for review October 29, 2014 and accepted December 15, 2014.

Published online December 22, 2014
10.1021/nn5061805

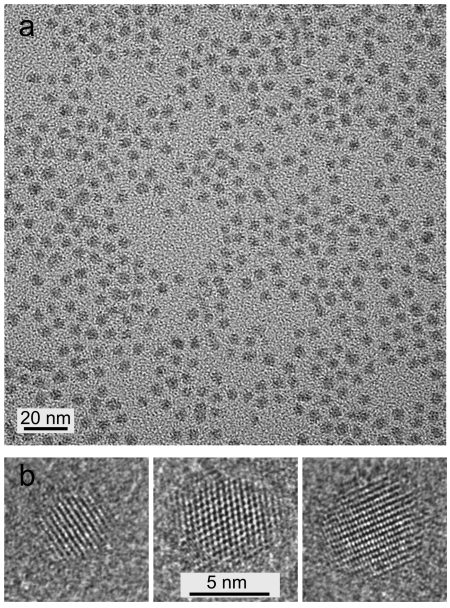

Figure 1. (A) Low-magnification TEM image of InSb nanocrystals. (B) High-resolution TEM images of several InSb NCs with different sizes, imaged along different crystal axes.

whose positions depend on NC size. We compared the tunneling spectra with the positions of the electron energy levels calculated within effective mass approximation and found that the tunneling occurs through the eight lowest quantum confinement levels associated with *L*-critical point of Brillion zone.

RESULTS/DISCUSSION

Recently developed synthetic protocol enabled preparation of size-selected samples of crystalline nearly spherical InSb NCs shown in Figure 1A. High-resolution TEM images show that NCs are highly crystalline and usually do not contain extended structural defects like stacking faults (Figure 1B).

Topography of InSb QDs on Highly Ordered Pyrolytic Graphite (HOPG). A typical noncontact AFM topographic image of a monolayer of InSb QDs on HOPG is shown in Figure 2A. The average QD size is 6.5 nm, in agreement with TEM analysis. The dark background on the bottom part of the image is the substrate, and the InSb QDs are the near-spherical shaped objects with brighter color due to the height difference. The InSb QDs form a 2D array on the surface with local hexagonal packing. The array lacks long-range order due to the size dispersion of the InSb QDs.

Control over the InSb QD concentration and the volume of solution drop-casted on the substrate allowed us to achieve a very low coverage of individual isolated InSb QDs over the substrate. We were able to observe 2D arrays, small clusters, and single, isolated InSb QDs on the same sample. Figure 2B shows a noncontact AFM topographic image of an isolated InSb QD on the HOPG substrate. These QDs are not chemically attached to the substrate. We observed that the QDs are mobile at room temperature and tend to

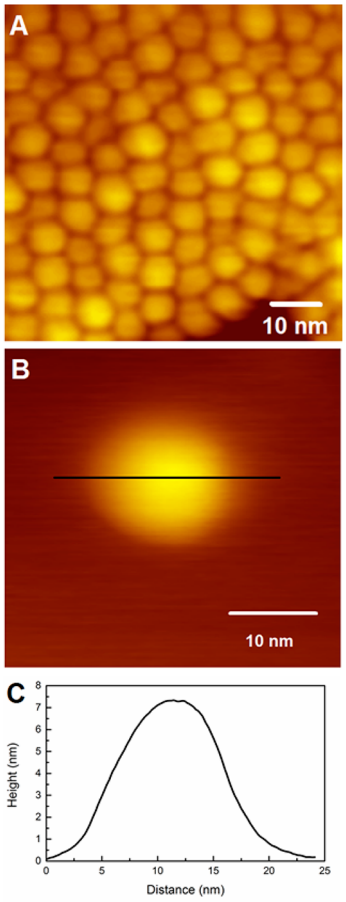

Figure 2. Topographic noncontact AFM image of InSb QDs on HOPG. (A) Topographic AFM image of a 2-D array of InSb QDs on HOPG. (B) Topographic AFM image of a single InSb QD on HOPG. (C) Height profile along the line indicated in (B). All images were obtained at $T = 25$ K.

diffuse toward the surface step edges. However, the mobility is minimized when the HOPG substrate is cooled at 25 K. Figure 2C shows the height profile of the QDs denoted in Figure 2B. The height of the QD measured by the AFM height profile (7.3 nm in Figure 2B) is considered to be the sum of the core of the QD and twice effective thickness of the capping molecule layer (~0.5 nm based on separation of individual InSb QDs in TEM images). The width of the QD, however, is larger than the height. This is because of the interaction between the moving tip and the QD. The same effects have been observed in previous reports.[17] In this study, we use the height measured by the AFM topographic images, corrected by the thickness of organic ligands (~1.0 nm) to determine the diameter of the QD.

Spectroscopy on Single InSb QDs on HOPG. Figure 3 shows a series of tunneling conductance spectra (d*I*/d*V* versus *V*) taken at $T = 25$ K on a single, isolated InSb QD with a diameter of 5.0 nm, which was measured from the height profile of the topographic AFM image shown in the inset of Figure 3. The features in the tunneling spectra are proportional to the local density of states (LDOS).[18] A series of tunneling resonance peaks

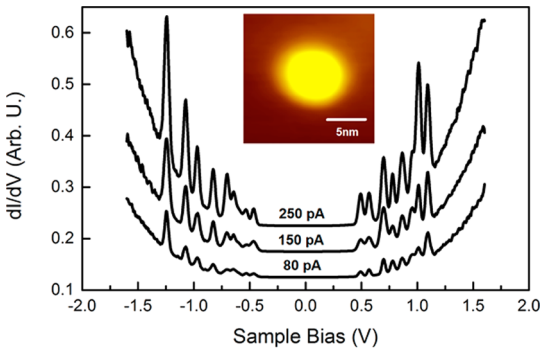

Figure 3. Tunneling spectra of a single 5.0 nm InSb QD at different tip-dot distances. All spectra were obtained by averaging about 40 individual, repeatable spectra taken at T = 25 K. The inset shows a topographic image of the InSb QD from which the spectra were taken. STS settings are set-point current 80, 150, and 250 pA at a bias voltage of 0.8 V. With increasing set-point current, the tip-QD distance decreases. The peak positions do not change but intensity increases with increasing set-point current.

are clearly observed on both positive and negative sample bias voltage sides of the spectrum. The peaks at positive sample bias voltage represent the electron tunneling through the conduction band states while the peaks at negative sample bias correspond to the hole tunneling through the valence band states of the measured QD. The separation between the peaks is determined by both the single-electron charging energy and the discrete level spacing.[19] The zero-current region at low-bias voltage corresponds to the QD energy band gap.

A series of peaks are resolved in the STS spectra of individual InSb QDs where differential conductance, dI/dV, is plotted vs applied bias voltage, V. Apart from having quantized energy levels, the QD is described as a continuous dielectric sphere placed in the external potential, ηV, where η is the fraction of the total external voltage that drops across the tip-QD tunnel junction. The energies of the single-particle states contributing to the tunneling current can be extracted from the experimental spectra if parameter η is obtained by numeric solution of the 3-D Laplace equation $\nabla^2 V = 0$. In the calculation, we use the following parameters: InSb dielectric constant of 16.8; capping molecule (oleic acid) dielectric constant of 3, capping molecule length is set to be 0.5 nm, tip-QD distance is set to be 1 nm, and the tip radius is 15 nm. With the above input, η is 0.68 and the result is plotted in Figure S1 (Supporting Information). The dependence of η on different parameters, such as the size of the QDs, capping molecule length and tip-dot distance, is also shown in Figure S1 (Supporting Information). We found that there is no strong dependence of η on these parameters.

To confirm reproducibility, we carried out the STS measurements on a single isolated InSb QD at different tip-QD distances, with other conditions kept the same. We varied the tip-QD distance by changing the set-point current between 80−250 pA at a bias voltage of 0.8 V. The larger the current set-point, the closer the tip is to the substrate and the higher tunneling rate from the tip to the QDs. As can be seen in Figure 3, changing the tunneling rate does not change the positions of the peaks in the measured spectra.

The observation of well-resolved multiplets of equidistant peaks in the STS spectra of InSb QDs suggests that tunneling through the conduction band states occurs in the shell-filling regime,[18] which happens when the carrier tunneling rate from tip to QD is much larger than the tunneling rate from QD to substrate. In this regime, carriers will accumulate in the QD and cause charging effects. For the QD shown in Figure 3, at positive bias side of the STS spectrum, a set of two peaks lies at +0.6 V separated by ~80 mV, followed by a larger separation and a group of six nearly equidistant peaks, also separated by ~80 mV. The first doublet can be assigned to the lowest conduction orbital that has S symmetry and spacing between the two peaks is $E_c(e) = \eta V \sim$ 55 meV, which is the single-electron charging energy. The observed $E_c(e)$ value corresponds to the charging energy of an isolated 5 nm conducting sphere embedded in a medium with effective dielectric constant of about 5, which is larger than the dielectric constant of organic ligands ($\varepsilon \sim 3$). We attribute this difference to the screening effect of substrate and tip. The nature of sextuplet will be discussed in depth below.

In contrast to the conduction band part of the STS spectra, the tunneling through the valence bands at negative bias voltage is more complicated. We think that the first doublet with a spacing of 48 meV, which is close to the E_c value observed for electrons, is the first level of the highest occupied orbit. Indeed, although the highest hole level in ideal spherical InSb NCs has total momentum 3/2 and is 4-fold degenerate state, this level is practically always split into two sublevels with momentum projection $M = \pm 1/2$ and $M = \pm 3/2$. This splitting can be connected with small deviation of the NC shape (oblate or prolate shape) from a sphere.[20] The doublet peak structure of the tunneling spectra is the result of charging of this two state level. The next doublet peaks at larger negative bias show spacing much larger than $E_c(h)$ because in addition to the charging energy we need to add the splitting energy between states $|M| = 3/2$ and $|M| = 1/2$. The other explanation could be that all hole tunneling occurs in the shell tunneling regime and we observe one peak per state. At the high negative bias cotunneling involving both hole and electron levels can complicate the STS spectra.

The zero-conductance region is the band gap, showing zero LDOS, plus twice the electron-charging energy. One can therefore calculate the band gap of InSb QDs from the tunneling spectra by first subtracting E_c from the measured spacing between the lowest conduction band and the highest valence band peaks and then multiplying this value by a conversion factor, which is discussed in the modeling section.

Size-Dependent Study of Electronic States of InSb and InAs QDs. The ability to vary the size of InSb provides an

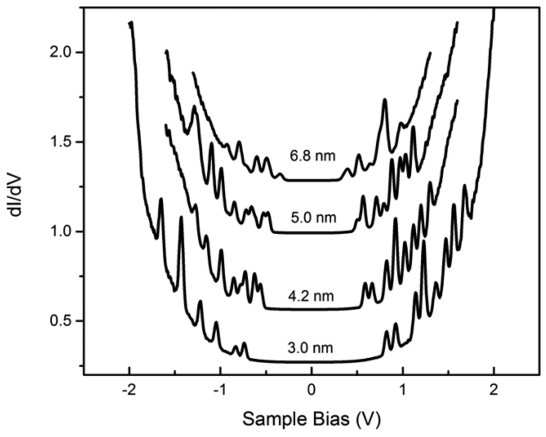

Figure 4. Tunneling spectra of InSb QDs with the diameters of 3.0, 4.2, 5.0, and 6.8 nm. Set-point currents were 70−90 pA, and bias voltages were between 0.6 and 0.8 V. The zero-conductance gap and the energy level separations increase as the size of the QDs decrease due to the quantum confinement effect. All spectra were taken at T = 25 K.

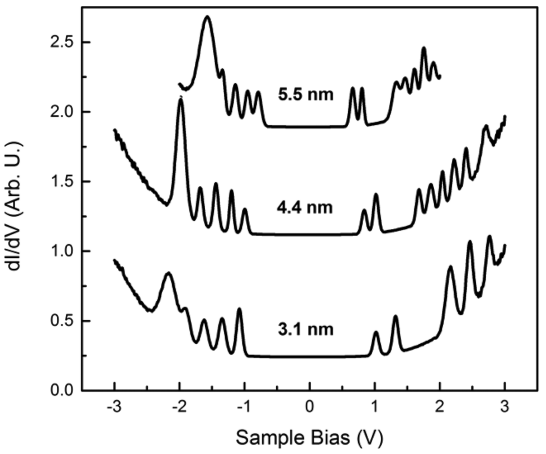

Figure 5. Tunneling spectra of InAs QDs with diameters of 3.1, 4.4, and 5.5 nm. Set-point currents were 80−90 pA, and bias voltages were between 0.6 and 0.8 V. The zero-conductance gap and the energy level separations increase as the size of the QDs decrease due to quantum confinement. All spectra were taken at T = 25 K.

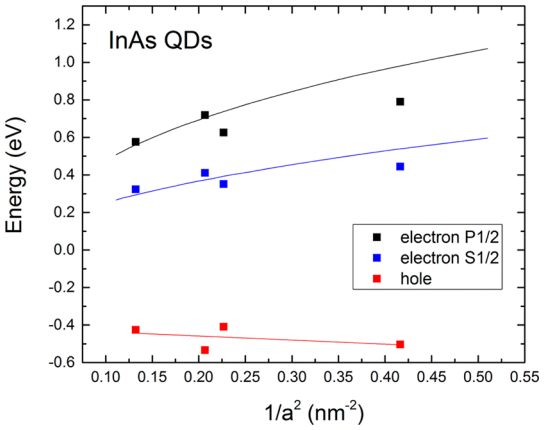

Figure 6. Experimental and simulated size dependence of the energy states of InAs QDs. The filled squares are experimental data. The solid blue and black lines show the theoretical dependences of electron energy levels on InAs QD size. The red solid line is not the calculated energy but guide to eye.

opportunity to conduct size-dependent studies of the electronic states of InSb QDs. Figure 4 shows a group of spectra corresponding to several single InSb QDs with core diameters of 3.0, 4.2, 5.0, and 6.8 nm, confirmed by their height profiles taken from the AFM images and corrected for the size of the ligands. Each spectrum is an average of 50 spectra at the same position of the same QD to improve signal-to-noise ratio. Resonance peaks are clearly observed at both positive and negative bias voltage for all spectra. All spectra have two groups of peaks on the positive-bias side. The first is a doublet, and the second has a 6-fold multiplicity. Both the spacing between the two groups and the spacing of peaks within the multiplet, as well as the HOMO−LUMO band gap, increase with decreasing QD diameter.

InAs is another member of the III−V semiconductor family. InAs QDs are expected to have similar electronic structures to InSb QDs. Banin *et al.* previously published STS of InAs QDs.[9] We are going to compare our data with previous results to verify consistency of our experimental procedures and theoretical analysis. Figure 5 shows a set of tunneling spectra of InAs QDs with diameters of 3.1, 4.4, and 5.5 nm. The data are quantitatively similar to the spectra shown in ref 9. This also proves that the spectra of InSb QDs under similar measuring conditions correctly reflect the electronic structure of InSb QDs.

Electronic Structure of InAs and InSb QDs. We first calculated the 1S and 1P electron energy levels for InAs QDs. Figure 6 compares experimental and simulated data showing clear agreement between the experimental and theoretical results for InAs QDs. Comparison between theory and experiment will be further used to explain the STS spectra and investigate the energy states in InSb QDs.

If we set the zero reference point of the potential and all energies at the grounded tip, the total electrostatic energy of q electrons in a QD is given by

$$H = -qe\eta V + \frac{1}{2}E_c q^2$$

where e is the (positive) elementary charge and E_c is the charging energy. The number of electrons populating the QD in a given bias is found by minimizing the Hamiltonian, $dH/dq = 0$. This gives the relation $qE_c = e\eta V$, which means that the additional energy, ΔE (or potential ΔV), required to inject an extra electron into the QD is $\Delta E = e\eta\Delta V = E_c$. With this information, the positions of the experimental dI/dV peaks can be connected with the single-particle state energies. For example, the first two dI/dV peaks appearing at voltages V_1 and V_2 are connected with the energy of the doubly degenerate ground-state S-electron by

$$e\eta V_1 = E_{S1/2} + E_c$$

$$e\eta V_2 = E_{S1/2} + 2E_c$$

One can see that the charging energy can be obtained, for example, from the distance between the first two peaks as $E_c = e\eta(V_2 - V_1)$, which in turn allows one to find the energy levels E_S, E_P. For example, if the second energy level has P symmetry, the tunneling peaks are expected at the following voltages:

$$e\eta V_3 = E_{P1/2} + 3E_c$$

$$e\eta V_4 = E_{P1/2} + 4E_c$$

$$e\eta V_5 = E_{P3/2} + 5E_c$$

$$e\eta V_6 = E_{P3/2} + 6E_c$$

$$e\eta V_7 = E_{P3/2} + 7E_c$$

$$e\eta V_8 = E_{P3/2} + 8E_c$$

The experimental STS spectra of the conduction band clearly show 8 peaks when positive voltage is applied which describes the electron tunneling current. The peaks, in turn, can be seen to fall into two distinct groups of two and six peaks, which intuitively suggests that the peaks originate from the 2-fold degenerate S-level and 6-fold degenerate P-level of the quantum-confined electron. Indeed, the two single-particle energy levels have been extracted from the experimental data using the above equations as shown in Figure 7.

It can be seen, however, that the energy spacing between these two energy levels is much smaller than the expectation, based on the general result of the effective mass approximation, that the S−P levels spacing should be on the order of the S-level confinement energy. To demonstrate the correctness of this statement, we calculated the size dependence of the first two electron states in the Γ-point of the first Brillouin zone of InSb QD using the eight-band $\mathbf{k}\cdot\mathbf{p}$ model.[21] The calculated dependencies, shown by black curves in Figure 7, demonstrate that although the calculated 1S electron level describes quite well the experimental size dependence of the ground electron state, the calculated 1P electron level is well above the second electron level observed in the STS spectra of InSb QDs.

In order to understand the origin of these transitions, we extrapolated the experimental size dependence of the lowest electron level plotted vs $1/a^2$ (a is the QD radius) to $1/a^2 \rightarrow 0$, which corresponds to bulk behavior. The experimental data have an almost linear dependence and gives the conduction band energy located ~140 meV above the bottom of the conduction band at the Γ-point of the Brillouin zone. From the slope of the $1/a^2$ experimental dependence, using a parabolic one-band model, we extracted the electron effective mass of the carriers as $m^* = 0.6m_0$.

This observation suggests the possibility that the electron tunneling may occur *via* the conduction band valley located at the *L*-point of the Brillouin zone. This valley indeed has a large effective mass and is higher in energy than the Γ-point conduction band edge. Using the extracted values of the conduction band offset and the effective mass, we calculate the energies of the two first electron levels in the *L*-valley, shown by red curves in Figure 7. We see again, however, that the energy difference between the two calculated levels is larger than the experimental difference. This raises the question what is the origin of the first excited 6-fold degenerate level observed in experiment.

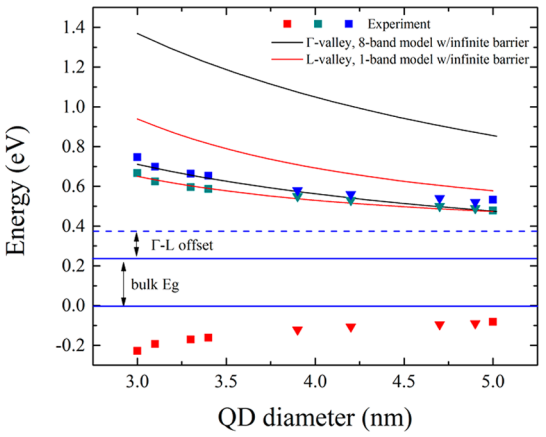

Figure 7. Size-dependence of the single-particle energy levels of carriers in InSb QDs. Square symbols: the experimental values extracted from the STS measurements taken from single InSb QDs isolated on HOPG. Triangular symbols: the experimental values extracted from the STS measurements taken from single InSb QDs embedded in an inert matrix of smaller CdSe NCs. The sizes are estimated by adding the height difference between of InSb QDs and surrounding CdSe QDs to the average size of CdSe QD islands. Black curves: two lowest Γ-point electron levels calculated within the 8-band effective mass model (ref 21). Red curves: two lowest *L*-point electron levels calculated with one-band parabolic model using a Γ − *L* offset of 140 meV and $m_L = 0.6m_0$. The conduction and valence band edges of bulk InSb at the Γ-point of the first Brillouin zone are shown by horizontal solid lines. The position of *L*-valley of the conduction band in bulk InSb extracted from the experimental size-dependence is shown by dashed line.

The answer may be connected with the fact that there are four equivalent *L*-valleys in the first Brillouin zone of InSb. As a result, there are four 1S electron levels connected with *L*-valleys where we can put generally eight electrons, consistent with our experimental observation. The degeneracy of the states in the different *L*-valleys is lifted by the intervalley mixing. Although we cannot calculate the magnitude of the intervalley interaction, ξ, in spherically shaped NCs it is the same for all four valleys. The intervalley mixing connected with the finite size of the NC is small and can be considered perturbatively. This leads to the following equations describing the intervalley coupling

$$EC_1 = -\xi(C_3 + C_4 + C_2)$$

$$EC_2 = -\xi(C_3 + C_4 + C_1)$$

$$EC_3 = -\xi(C_4 + C_1 + C_2)$$

$$EC_4 = -\xi(C_1 + C_2 + C_3)$$

where E is the shift of the 1S level and the coefficients $C_{1,2,3,4}$ describe the magnitude of the contributions of each one of the four valleys to the final states. Summing up all equations, or extracting line from line in the above equations, one gets a singlet level with

$$E = -3\xi$$

where the wave function has equal contribution from each valley. Above the singlet level there should be a six-degenerate triplet level with wave functions, $C_1 - C_2$ and $C_3 = C_4 = 0$; $C_2 - C_3$ and $C_1 = C_4 = 0$; and $C_3 - C_4$ and $C_1 = C_2 = 0$. The energy of this triplet level should be

$$E = \xi$$

These analyses show that the small value of the observed splitting, 4ξ, and observed level degeneracy (2 and 6) are consistent with tunneling occurring through the lowest 1S electron levels of the *L*-valleys.

This interpretation of the tunneling experiments, however, implies that at the temperature of the experiment (25K) the $\Gamma-L$ offset is significantly smaller than the room temperature value of 510 meV.[22] Our value of 140 meV is consistent with the observation that the oscillatory magnetoabsorption spectra of bulk InSb crystals in ref 23 begin to lose structure at the energies of ~150−200 meV above the Γ-point conduction band bottom at 1.8 K. This is in line with the previous studies showing that the energy gap between direct and indirect valleys in III−V semiconductors decreases with reduction of lattice constant at low temperature or high pressure.[24]

Our experimental data suggest strongly that in the low temperature STS measurements of the InSb QDs, the electrons tunnel *via* the *L*-point conduction band states. This could occur because the tunneling through the *L*-point of Brillioun zone is more efficient than the tunneling through the Γ-point. A more likely explanation of the observed phenomenon, however, is connected with direct−indirect transition, which could occur in small size InSb NCs. Indeed, due to the small effective mass of the electron at the Γ-point, $m_{e\Gamma} = 0.0139m_0$, the ground 1S level shifts much faster to the higher energy than the 1S level of the *L*-point of the Brillouin zone and can have larger energy than the latter one in small size NCs. Although we do not know the effective masses of the electron in the *L*-valley and the conduction band offset between the Γ and *L*-valleys at 25 K, our approximate calculations show that this direct-indirect transition should happen in NCs with radius smaller than 5 nm (see Figure 7). We also note here that direct−indirect transitions should be very difficult to see in absorption spectra of InSb NCs. After the transition, the absorption spectra of InSb NCs may continue to show the sharp exciton peak connected with an exciton in the Γ-point of Brillouin zone superimposed on the weak broad background connected with indirect band gap transitions. This type of absorption spectrum has been seen in bulk Ge, where the direct band gap is just 100 meV above the indirect gap.[25]

Our STS study strongly suggests the presence of proximal electronic states in the Γ- and *L*-valleys of strongly quantum-confined InSb QDs. This observation complements the recent study of the picosecond dynamics in transient absorption spectra of colloidal InSb QDs.[26] There we observed unusual ultrafast carrier dynamics that could be explained by transfer of carriers between two optical transitions of comparable energy within a manifold involving multiple coupled conduction band states. Combined with the STS study reported here, we now have growing evidence of the important role of previously ignored multivalley effects in strongly quantum-confined semiconductor QDs.

CONCLUSIONS

Single InSb QDs were investigated by AFM and tunneling spectroscopy. We have observed clear resonance tunneling peaks on both positive and negative sample bias tunneling conditions. This reveals the conduction (positive bias side) states and valence (negative bias side) states of InSb QDs. Peak splitting due to charging is observed, proving the tunneling is in a shell-filling condition. A series of InSb QDs with different diameters (3 to 7 nm) have been studied using STS. Decreasing the size of the QDs leads to larger band gap and energy spacing between conduction and valence levels. Similar experiments have been carried out on InAs QDs, another member of the III−V semiconductor family. The difference in the tunneling spectra between InAs and InSb QDs indicates that the tunneling process is different. Theoretical calculations strongly suggest that the electron tunneling of InSb QDs occurs through quantum confined levels connected with *L*-points of Brillouin zone. This is the first time such a tunneling process has been observed for colloidal III−V QDs.

METHODS

Nanocrystal Synthesis. To synthesize InSb NCs, the stock solution of $LiBEt_3H$ (5.0 mL, 2.0 M) and $InCl_3/Sb[N(Si(Me)_3)_2]_3$ (0.8 mmol for each) were injected in an immediate sequence into 12.0 mL of anhydrous oleylamine at room temperature under vigorous stirring. The mixture was heated up to 260 °C with ramping rate of ~10 °C/min and annealed for ~20 min. The black colloidal solution was then cooled down naturally to room temperature and transferred into a glovebox for the postsynthetic procedures.

Twenty milliliters of anhydrous toluene and 5.0 mL of anhydrous oleic acid were added to the solution to dilute the concentration and partially replace oleylamine ligand. A significant amount of viscous precipitate was formed. Addition of

toluene (~100 mL) was used to wash the precipitate to extract NCs until nearly clear supernatant was obtained. The as-synthesized InSb NCs had a broad size distribution (>12%). Multiple fractions of monodisperse NCs can be obtained with a careful size selective precipitation approach using toluene and acetonitrile as the solvent and nonsolvent, respectively.

For the synthesis of InAs NCs, 1.0 mL stock solution of $InCl_3$ (1.1 mmol) and $(TMS)_3As$ (0.7 mmol) in TOP was swiftly injected into 2.0 g of TOP at 300 °C under vigorous stirring. The solution was then annealed at 260 °C. Two consecutive injections of stock solution were performed dropwise to make big NCs (~5 nm in diameter). When the desired size was reached, the solution was naturally cooled to room temperature and transferred into a glovebox for washing. Size selection with toluene and ethanol as the solvent and nonsolvent were used to prepare monodisperse NCs. Additional details on NC synthesis are provided in the Supporting Information.

Sample Preparation for AFM and STS Measurements. The electronic structure of individual InSb QDs was measured after their isolation on freshly cleaved highly ordered pyrolytic graphite (HOPG). A size series of InSb QDs (having mean core diameters of 3.2, 4.0, 4.7, and 6.5 nm) capped with oleylamine and oleic acid were synthesized. The 3.2 and 4.0 nm InSb QDs were isolated by using very dilute InSb solutions, while the 4.7 and 6.5 nm InSb QDs were dispersed in a matrix of smaller CdSe QDs (~4.5 and 3.5 nm, respectively). CdSe QDs were used as an inert matrix to isolate single InSb QDs and small InSb QD clusters. The details will be discussed below. The CdSe QDs were passivated with octadecylphosphonic acid (ODPA) and trioctylphoshphine oxide (TOPO). The diameters of the QDs were determined by transmission electronic microscopy (TEM) and UV−vis optical spectroscopy.

The QD samples (both pure InSb and InSb/CdSe mixtures) were prepared by drop casting dilute colloidal solutions in 9:1 v:v hexane:octane on freshly cleaved HOPG. Control over the concentration ratio of InSb to CdSe led to submonolayer surface coverage with predominately isolated InSb QDs surrounded by arrays of CdSe QDs. All sample preparation took place inside a nitrogen filled glovebox using anhydrous solvents. The samples were transferred to an airtight nitrogen-filled container until insertion into the ultrahigh vacuum (UHV) system.

Noncontact AFM Measurements. Immediately after sample preparation, the sample was loaded into the ultrahigh vacuum (UHV) system with a base pressure less than 5×10^{-11} Torr. AFM measurements were made with a commercial variable-temperature UHV scanning probe microscopy (SPM) system (Model 350, RHK Technology, Inc.), which allowed us to switch between STM and AFM in UHV. The AFM tips (Nanoscience Inc.) were coated with Pt for STS measurements, with a radius less than 15 nm. All AFM measurements were done in noncontact mode. The sample was measured without preannealing. Low-temperature imaging was conducted at $T = 25$ K in UHV.

STS Measurements. In our STS studies, the samples were cooled to 25 K in UHV. However, the metal-coated AFM tip was not actively cooled and thus remained below room temperature but higher than that of the sample. This limited energy resolution to about 10 meV. The STS measurements were conducted at preselected points, usually the center of an individual QD, within an AFM image. After moving the metal-coated conductive AFM tip to the preselected point, the feedback loop was disconnected and STM mode selected to read the tunneling current. All spectra were taken at 25 K with a set-point current ranging from 50 pA to 200 pA at a bias voltage of 0.8 V. The tunneling current (I) and conductance (dI/dV) were measured simultaneously. A lock-in amplifier was used to improve signal-to-noise ratio. The typical parameters of the lock-in amplifier were 1000−2000 Hz in frequency, 20−40 mV in amplitude. We took multiple spectra to verify reproducibility and averaged 50−100 dI/dV spectra to improve the signal-to-noise ratio. The conductance spectra were also obtained by numerically differentiating the current−voltage curves. The spectra were compared with those taken without the lock-in amplifier. The results are consistent with each other but the signal-to-noise ratio was significantly improved by using lock-in detection.

Between 50 and 100 $I-V$ and dI/dV spectra were measured on each QD and checked for reproducibility. Generally, the tunneling spectra were very reproducible, and we did not observe any significant peak shift. However, in some cases, we found that after taking spectra for a while the resonant tunneling peaks suddenly disappeared leaving either featureless spectra or big spikes. We attribute this observation to temporary changes of the tip condition due to ligand contamination. After a quick flip of the bias voltage (from −5 V to +5 V) to clean the AFM tip we could recover the same reproducible spectra again.

Conflict of Interest: The authors declare no competing financial interest.

Acknowledgment. S.J.S. and D.T. acknowledge support from the NSF MRSEC at The University of Chicago, Award Nos. DMR 08-20054 and DMR 14-20709. S.J.S. acknowledges support from the DURIP program, Award No. AFOSR-FA9550-09-1-0411. A.L.E. acknowledges financial support of the Office of Naval Research (ONR) through the Naval Research Laboratory Basic Research Program. The work on synthesis and characterization of InSb QDs was also supported by DOD ONR Award No. N00014-13-1-0490 and NSF under Award No. DMR-1310398. D.V.T. further thanks the Keck Foundation for support. E.L. and R.V. acknowledge support from the Israel Science Foundation (Project Nos. 1009/07 and 1425/04), the USA−Israel Binational Science Foundation (No. 2006-225), and the Israel Council for High Education - Focal Area Technology (Project No. 872967).

Supporting Information Available: Further information on dot synthesis as well as the results from the 3-D Laplace equation solutions for InSb dot/tip systems. This material is available free of charge *via* the Internet at http://pubs.acs.org.

REFERENCES AND NOTES

1. Alivisatos, A. P. Perspectives on the Physical Chemistry of Semiconductor Nanocrystals. *J. Phys. Chem.* **1996**, *100*, 13226.
2. Manna, L.; Scher, E. C.; Alivisatos, A. P. Synthesis of Soluble and Processable Rod-, Arrow-, Teardrop-, and Tetrapod-shaped CdSe Nanocrystals. *J. Am. Chem. Soc.* **2000**, *122*, 12700.
3. Müller, J.; Lupton, J. M.; Lagoudakis, P. G.; Schindler, F.; Koeppe, R.; Rogach, A. L.; Feldmann, J.; Talapin, D. V.; Weller, H. Wave Function Engineering in Elongated Semiconductor Nanocrystals with Heterogeneous Carrier Confinement. *Nano Lett.* **2005**, *5*, 2044.
4. Murray, C. B.; Kagan, C. R.; Bawendi, M. G. Synthesis and Characterization of Monodisperse Nanocrystals and Close-packed Nanocrystal Assemblies. *Annu. Rev. Mater. Sci.* **2000**, *30*, 545.
5. Redl, F. X.; Cho, K. S.; Murray, C. B.; O'Brien, S. Three-dimensional Binary Superlattices of Magnetic Nanocrystals and Semiconductor Quantum Dots. *Nature* **2003**, *423*, 968.
6. Chen, Z.; O'Brien, S. Structure Direction of II-VI Semiconductor Quantum Dot Binary Nanoparticle Superlattices by Tuning Radius Ratio. *ACS Nano* **2008**, *2*, 1219.
7. Murray, C. B.; Sun, S.; Gaschler, W.; Doyle, H.; Betley, T. A.; Kagan, C. R. Colloidal Synthesis of Nanocrystals and Nanocrystal Superlattices. *IBM J. Res. Dev.* **2001**, *45*, 47.
8. Liu, W.; Chang, A. Y.; Schaller, R. D.; Talapin, D. V. Colloidal InSb Nanocrystals. *J. Am. Chem. Soc.* **2012**, *134*, 20258.
9. Banin, U.; Cao, Y.; Katz, D.; Millo, O. Identifcation of Atomic-like Electronic States in Indium Arsenide Nanocrystal Quantum Dots. *Nature* **1999**, *400*, 542.
10. Millo, O.; Katz, D.; Cao, Y.; Banin, U. Scanning Tunneling Spectroscopy of InAs Nanocrystal Quantum Dots. *Phys. Rev. B* **2000**, *61*, 16773.
11. Banin, U.; Millo, O. Tunneling and Optical Spectroscopy of Semiconductor Nanocrystals. *Annu. Rev. Phys. Chem.* **2003**, *54*, 465.
12. Maltezopoulos, T.; Bolz, A.; Meyer, C.; Heyn, C.; Hansen, W.; Morgenstern, M.; Wiesendanger, R. Wave-function Mapping of InAs Quantum Dots by Scanning Tunneling Spectroscopy. *Phys. Rev. Lett.* **2003**, *91*, 196804.

13. Bakkers, E. P. A. M.; Hens, Z.; Zunger, A.; Franceschetti, A.; Kouwenhoven, L. P.; Gurevich, L.; Vanmaekelbergh, D. Shell-Tunneling Spectroscopy of the Single-Particle Energy Levels of Insulating Quantum Dots. *Nano Lett.* **2001**, *1*, 551.
14. Hens, Z.; Grandidier, B.; Deresmes, D.; Allan, G.; Delerue, C.; Stievenard, D.; Vanmaekelbergh, D. Evolution of the Density of States on Going from a Two- to a Zero-Dimensional Semiconductor. *Europhys. Lett.* **2004**, *65*, 809.
15. Hens, Z.; Vanmaekelbergh, D.; Stoffels, E. J. A. J.; van Kempen, H. Effects of Crystal Shape on the Energy Levels of Zero-Dimensional PbS Quantum Dots. *Phys. Rev. Lett.* **2002**, *88*, 236803.
16. Liljeroth, P.; Zeijlmans van Emmichoven, P. A.; Hickey, S. G.; Weller, H.; Grandidier, B.; Allan, G.; Vanmaekelbergh, D. Density of States Measured by Scanning-tunneling Spectroscopy Sheds New Light on the Optical Transitions in PbSe Nanocrystals. *Phys. Rev. Lett.* **2005**, *95*, 086801/1.
17. Jdira, L.; Overgaag, K.; Stiufiuc, R.; Grandidier, B.; Delerue, C.; Speller, S.; Vanmaekelbergh, D. Linewidth of Resonances in Scanning Tunneling Spectroscopy. *Phys. Rev. B* **2008**, *77*, 205308.
18. Liljeroth, P.; Jdira, L.; Overgaag, K.; Grandidier, B.; Speller, S.; Vanmaekelbergh, D. Can Scanning Tunnelling Spectroscopy Measure the Density of States of Semiconductor Quantum Dots? *Phys. Chem. Chem. Phys.* **2006**, *8*, 3845.
19. Porath, D.; Levi, Y.; Tarabia, M.; Millo, O. Tunneling Spectroscopy of Isolated C60 Molecules in the Presence of Charging Effects. *Phys. Rev. B* **1997**, *56*, 9829.
20. Efros, Al. L.; Rodina, A. V. Band-Edge Absorption and Luminescence of Nonspherical Nanometer-Size Crystals. *Phys. Rev. B* **1993**, *47*, 10005.
21. Efros, Al. L.; Rosen, M. Quantum Size Level Structure of Narrow-Gap Semiconductor Nanocrystals: Effect of Band Coupling. *Phys. Rev. B* **1998**, *58*, 7120.
22. *Handbook Series on Semiconductor Parameters*; Levinshtein, M., Rumyantsev, S., Shur, M., Eds.; World Scientific: Singapore, 1996.
23. Efros, Al. L.; Kanskaya, L. M.; Kokhanovskii, S. I.; Seysyan, R. P. Indium Antimonide Energy Band Parameters Derived from Diamagnetic Exciton Spectra. *Solid State Commun.* **1982**, *43*, 613.
24. Yu, P. Y.; Welber, B. High Pressure Photoluminescence and Resonant Raman Study of GaAs. *Solid State Commun.* **1978**, *25*, 209.
25. Asnin, V. M.; Rogachev, A. A. Exciton Absorption in Doped Germanium. *Phys. Status Solidi* **1967**, *20*, 755.
26. Chang, A. Y.; Liu, W.; Talapin, D. V.; Schaller, R. D. Carrier Dynamics in Highly Quantum-Confined, Colloidal Indium Antimonide Nanocrystals. *ACS Nano* **2014**, *8*, 8513.